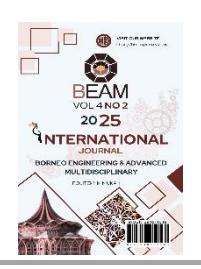


# Borneo Engineering & Advanced Multidisciplinary International Journal (BEAM)

Volume 4, Issue 2, November 2025, Pages 11-18



# Design and Development of Modular and Small-Scale Needle Punching Mechanism Non-Woven Machine

Raynabelle Emilia Raymond<sup>1</sup>\*, Muhammad Farid Shaari<sup>1</sup>, Yoganand Mohand<sup>1</sup>, Aimi Syamimi Ab Ghafar<sup>1</sup>, Muhammad Aqil Ramlan<sup>2</sup>, Mohamad Amirul Aizat Hassan<sup>1</sup>

<sup>1</sup>Faculty of Engineering Technology, Universiti Tun Hussein Onn Malaysia, Pagoh Campus, Pagoh Higher Education Hub, 84600 Muar, Johor, Malaysia <sup>2</sup>Camwell Sdn. Bhd., No.12 & 14, Jalan Hasil 1, Kawasan Perindustrian Tampoi,81200 Johor Bahru, Johor, Malaysia

\*Corresponding author: raynabelleemilia@gmail.com Please provide an official organisation email of the corresponding author

# **Full Paper**

Article history
Received
7 May 2025
Received in revised form
8 July 2025
Accepted
27 August 2025
Published online
1 November 2025



#### **Abstract**

Natural fibers like cotton, coconut, and bamboo are finding new life in needle-punched non-woven fabrics, creating ecofriendly alternatives for applications ranging from car interiors to gardening mats. Regular testing is essential to ensure the quality of multi-fiber non-woven production. However, the current testing process often requires needle changes, which can be time-consuming. Therefore, this project aims to streamline the needle adjustment process. A small-scale prototype was developed to explore and understand structural aspects, conduct testing and simulations, gather valuable data on prototype behavior, and visually investigate the results. Finite Element Analysis (FEA) was conducted during the design stage to determine the Von Mises stress, strain, and displacement of the machine structure. Operational testing involved varying the needle punching speed at a fixed feed rate to study fiber entanglement formation. The needle punching speeds tested were 300 rpm, 200 rpm, 150 rpm, 100 rpm, and 60 rpm. Results showed that 300 rpm produced the finest fiber entanglement and yielded a smoother and more uniform surface appearance in the fabric. FEA simulation results indicated that under a needle punching force ranging from 3N to 9N, the Von Mises stress (1692.66 N/m), displacement (1.3703  $\times$  E-10 m), and strain (1.8395  $\times$  E-8) were within acceptable limits. Overall, results from the operational tests and simulation analysis demonstrate that the prototype performs effectively within failure limitation.

Keywords: - Non-woven, needle punching, needle punching prototype, bamboo-based fiber

Copyright © This is an open access article distributed under the terms of the Creative Commons Attribution License



### 1. Introduction

Non-woven felt or fabrics are used in disposable medical gowns, wipes, geotextiles, automotive interiors, and packaging. These materials serve healthcare, hygiene, construction, automotive, and consumer goods industries, proving its adaptability in a flexible and scalable modern industry (Ajmeri, J. R. & Ajmeri, C. J., 2016).

Fibrous webs, whether natural or synthetic, move smoothly into the machine-like dancers awaiting its turn. Sharp needles, acting as skilled performers, repeatedly plunge and withdraw, using its barbed tips to intertwine and bind the fibers into a unified structure (Paul et al., 2022a).

One of the essential mechanisms in non-woven process is needle punching. When the fiber fed into the needle punching area, sharp needles repeatedly plunge and withdraw, using its barbed tips to intertwine and bind the fibers into a unified structure (Paul et al., 2022a) In product development or research and development (R&D) section, optimization of different fiber composition always attempted by researchers to enhance final product quality and performance.

Fibers sizes and web thickness changes are uncertain. This situation demands frequent needle changes and would affects production time if the optimizing process is using similar machine in the production line. Hence, this project proposes a small scale non-woven machine for easy maintenance and needle replacement. The main aim of this

project was to investigate the reliability of the developed prototype. Modular needle punching mechanism was selected as the main concept of the solution. The other factors that being considered in this design including machine structure integrity against vibration during operation, kinematics as well as smoothness of link movements. Research works including Finite Element Analysis (FEA) simulation to determine the stability of machine structure, prototype fabrication and prototype testing using natural fiber. In this research, untreated bamboo fiber and polyester fiber composition was used to test the performance of the developed prototype.

#### 2. Literature Review

Fibers are long, flexible strands derived from natural sources like cotton and wool or synthetic materials such as polyester and nylon, valued for its strength, durability, and adaptability (Hill, 2019; Smith & Jones, 2020; McDonagh, 2016 & Kadolph & Langford, 2002). Nonwoven fabrics, produced by bonding fibers mechanically, chemically, or thermally, are widely used in healthcare, personal care, and geotextiles due to its cost-effectiveness and customizable properties (Hu, 2008 & Pourmohammadi, 2013). Usually, techniques which are spun bonding and melt blowing are used to enhance characteristics such as breathability and water resistance (Chapman, 2010). These fabrics are essential in applications requiring moisture control and air permeability, such as hygiene products and medical supplies (Albrecht et al., 2006 & Lawrence & Branson, 2001).

Needle punching, a key nonwoven fabric production method, interlocks fibers using barbed needles in a vertical motion, forming strong and stable textiles for carpets, upholstery, and geotextiles. Industrial machines stabilize vibrations to ensure smooth operation (Hearle & Hollingworth, 1998), and process steps such as batt formation and density control influence fabric characteristics (Ajmeri, J. R. & Ajmeri, C. J., 2016). Various machine types, from vertical looms to rotary looms and handheld devices, cater to different applications, with needle design playing a critical role in fiber entanglement and durability. Automation continues to enhance efficiency and sustainability in needle punching.

Finite Element Analysis (FEA) evaluates structural responses under various loading conditions by dividing them into smaller elements for precise assessment. Common in mechanical, civil, aerospace, and automotive engineering, FEA analyzes mechanical properties such as stress, strain, and deformation to identify high-stress areas and potential failure points (Callister & Rethwisch, 2018). Stress measures internal forces, strain quantifies deformation, and deformation assesses displacement caused by external loads. These properties influence material selection and performance in industries like construction and automotive (Ashby & Jones, 2012). Stress analysis predicts structural integrity and failure mechanisms (Huangfu et al., 2023), while strain testing helps determine material stiffness, elasticity, and failure

limits (Takagi & Yoshida, 2022). Understanding deformation is crucial for ensuring material strength, ductility, and stability in engineering applications.



Fig. 1: Non-woven formation zone (Paul et al., 2022b)

# 3. Methodology

The needle punching machine is constructed using motors, cranks, and shafts as its underlying mechanisms. The initial design was based on early ideas and concepts, with advancements made as the research progressed. Fabrication techniques are utilized in the machine's construction. The primary objective of building the modular needle punching machine is to provide a functional mechanism that supports further nonwoven fabric experiments. Additionally, the output of the observed nonwoven fabric sample will depend on the study of parameter optimization for the coarse coconut fiber nonwoven process.

#### 3.1 Machine Structure Design

The structure of needle punching machine consist of two primary component which is needle punching mechanism and the machine frame. The needle punching mechanism carries out the punching process and includes critical parts such as beds or plates, needle boards, and needles. During operation, the needles, positioned on the needle board, move vertically to interlock fibers. Meanwhile, the frame acts as the structural support system, ensuring stability and proper alignment of the needle punching mechanism, thereby enhancing the machine's efficiency and reliability. When the crank rotates, it moves the connecting rod, which pushes and pulls the slider along a linear path, resulting in a sinusoidal displacement relative to the crank's position. In an engine, the piston (or slider) compresses the air-fuel mixture, ignites the fuel, and transfers force back to the crankshaft through the connecting rod, producing rotational motion. A similar mechanism is utilized in the non-woven process, where a crank connected to a 12V DC motor drives the connecting rod. The connecting rod acts as both a linkage and a transformation element, converting the motor's rotary motion into reciprocating motion, causing the needle plate to oscillate vertically, as illustrated in Fig. 2.

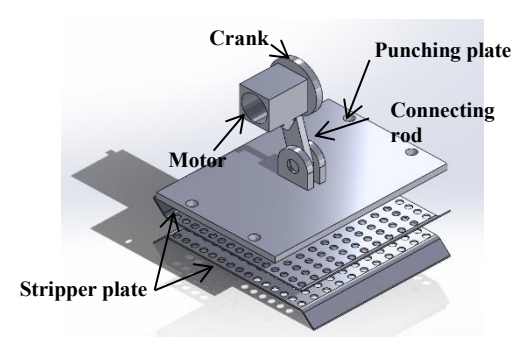


Fig. 2: Conceptual design model

Next, the crank mechanism was installed, incorporating a 12V DC motor that powered the connecting rod. As the motor rotated, the crank transferred motion to the rod, which in turn moved the slider along a linear path, producing a sinusoidal displacement. This mechanism was integral to the non-woven process, facilitating the conversion of rotary motion into reciprocating motion to drive the needle plate's up-and-down movement, as demonstrated in Fig. 3.

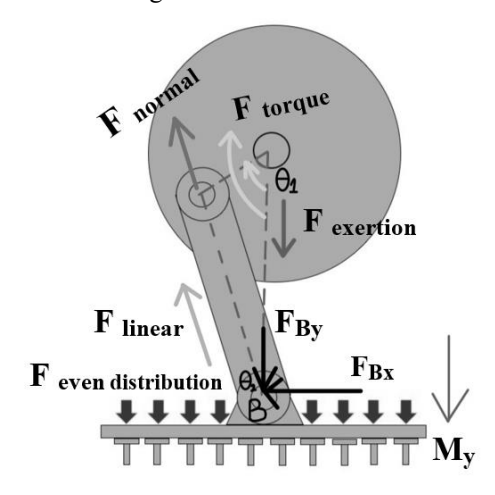


Fig. 3: Needle punching mechanism free body diagram

Calculating the force from a motor is essential to understand its ability to drive mechanical systems efficiently. The force generated by a motor is directly related to its torque and the radius at which the force is applied, influencing the overall performance of the system. In applications such as needle punching machines, motors convert electrical energy into mechanical motion, which is then transferred to components like crank mechanisms and connecting rods. Additionally, accurate force calculations help optimize the design by selecting appropriate materials, avoiding unnecessary weight, and ensuring energy efficiency. It also aids in preventing issues such as motor overloading or underperformance, ultimately improving the reliability and longevity of the system. The force from motor was calculated using equation (1) (Oriental Motor U.S.A. Corp., n.d.).

$$F_m = \frac{\mathrm{T}}{r} \tag{1}$$

Where  $F_m$  is force from motor in N, T is torque in N/m and r is radius of crank in m.

The mass of the punching plate needed to be calculated because it directly influenced the dynamic behaviour of the system. Since the plate was connected to the motor through a linkage mechanism, its mass affected the force required to move it and the overall energy consumption. A heavier plate required more force to accelerate and decelerate, increasing the load on the motor and potentially reducing efficiency. Additionally, excessive mass could cause imbalanced motion, leading to vibrations that might compromise stability and precision during operation. By determining the mass, the appropriate motor torque and linkage strength could be selected to ensure smooth and efficient movement. Proper mass calculation also helped prevent excessive wear on mechanical components, enhancing durability and performance. Equation (2) is used to calculate the mass of the punching plate.

$$m = \rho \times V \tag{2}$$

Where m is mass unit in kg,  $\rho$  represent density of punching plate and V is volume of punching plate unit in  $m^3$ .

#### 3.2 FEA Simulation

FEA simulation was conducted to validate the needle punching system design by analysing component stress, fatigue resistance, and motion synchronization using FEA Solidworks software. Motor speed was adjusted to regulate the punching frequency, creating different processing conditions. As the speed increased, the time per cycle decreased, leading to lower inertial forces due to reduced acceleration. The force exerted by the motor was calculated based on its speed, ensuring accurate parameter selection for different operating conditions. These force values were then used to form various parameter combinations, allowing an assessment of how different speed and force settings influenced performance. By systematically varying these parameters, optimal conditions for efficient operation and improved material processing could be identified. The selected motor speeds were 60, 100, 150, 200, and 300 rpm, resulting in a total of five sample combinations. The relation between motor speed and force motor as calculated in equation (1) is summarize in Table 1.

Table 1: Samples of parameter combination

Motor Speed (rpm)	Force (N)	Torque (Nm)
60	8.825	0.3530
100	7.110	0.2844
150	4.903	0.1961
200	3.678	0.1471
300	2.943	0.1177

In FEA simulation, determining angular velocity and angular acceleration is crucial for calculating centrifugal force, as these factors describe a component's rotational motion. Centrifugal force depends on mass, the rotational radius, and the square of angular velocity. Without angular velocity, the outward force acting on rotating parts cannot be accurately determined.

Moreover, angular acceleration must be considered to account for variations in rotational speed over time. When a body undergoes rotational acceleration, dynamic forces which includes inertial and reactive forces must be analysed to ensure accurate simulation results. Incorporating both angular velocity and angular acceleration enhances the accuracy of force predictions, contributing to improved design optimization and reliability analysis. Equation (3) is used to find the value of angular velocity while equation (4) is used to find the value of angular acceleration (Urone & Hinrichs, 2016).

$$\omega = 2\pi \times n \tag{3}$$

Where  $\omega$  is angular velocity unit in rad/s and n is rotational speed unit in sec.

$$\alpha = \frac{\omega}{t} \tag{4}$$

Where  $\alpha$  is angular acceleration unit in rad/s<sup>2</sup>,  $\omega$  is angular velocity unit in rad/s and t is time unit in sec.

The Table 2 shows an increase in rotational speed led to a proportional rise in both angular velocity and angular acceleration. This pattern was anticipated, as shown in Fig. 4, as higher rotational speeds caused a greater rate of change in angular velocity over time. These calculations played a significant role in analysing the system's dynamic behaviour, particularly in evaluating centrifugal forces and enhancing the mechanical design for improved efficiency and stability.

Table 2: Data calculation of angular velocity and angular acceleration

Motor Speed (rpm)	Angular Velocity, ω (rad/s)	Angular Acceleration, $\alpha$ (rad/ $s^2$ )
60	6.283	0.314
100	10.472	0.524
150	15.708	0.785
200	20.944	1.047
300	31.415	1.571

Based on Fig. 4 the graph shows distinct correlation between motor speed (rpm), angular velocity ( $\omega$ ), and angular acceleration ( $\alpha$ ). As the motor speed increases from 60 to 300 rpm, the angular velocity exhibits a proportional rise, signifying a linear relationship between these variables. Furthermore, the graph indicates that angular acceleration also increases with motor speed; however, this relationship is nonlinear. The curvature of the red line implies that at higher rotational speeds, the rate of change in angular velocity becomes more significant, resulting in a more rapid increase in angular acceleration.

In summary, the graph confirms that an increase in motor speed not only elevates angular velocity but also considerably intensifies angular acceleration.

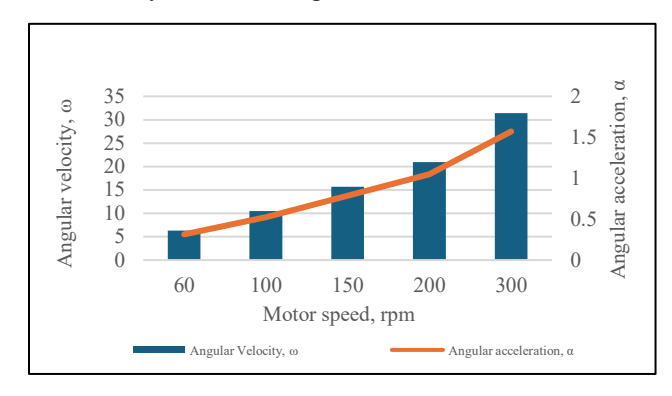


Fig. 4: Relationship between rotational speed, angular velocity and angular acceleration

The final step in the FEA pre-processing for the needle punching prototype involved setting the mesh. A blended curvature-based mesh was applied in this simulation to enhance both accuracy and computational efficiency by adapting the mesh density based on the geometry's curvature. This approach allowed finer mesh elements in high-curvature regions and coarser elements in flatter areas, optimizing the overall element distribution. The total number of mesh elements was 178,803, with the smallest element size being 1.15983 mm. Detailed mesh information is presented in Table 3.

Table 3: Mesh information

Criteria	Value / Type
Mesh Type	Solid Mesh
Mesher Used	Blended curvature-based mesh
Maximum element size	23.1966 mm
Minimum element size	1.15983 mm
Total nodes	351746
Total elements	178803

# 3.3 System Design

As shown in Fig. 3, the critical part of this mechanism is the movable rotational-to-linear conversion link structure. A 12 VDC motor with higher torque was selected to drive the cam that linked to the needle plate through free arm. Motor actuation was controlled using PLC (OMRON CP1L). Two different power supplies were utilized in this system which were 24VDC to power the PLC and switches, and 12VDC to power the drive motor. As two different power supply were installed in the system, relay was used to trigger drive motor actuation from PLC. Speed controller was applied to set the drive motor speed. The system setup is shown as in Fig. 5.

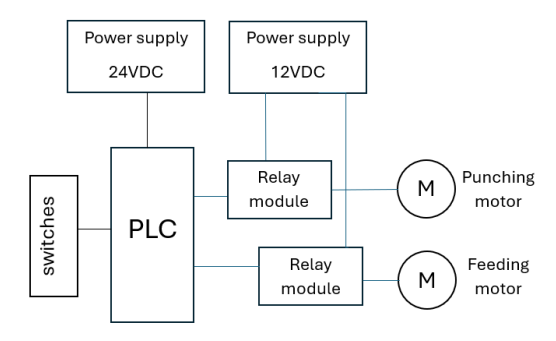


Fig. 5 System setup

#### 3.4 System Testing

System was tested to verify the functional components of the prototype. When "Start" button was pressed, the PLC successfully activated the relay module, switching on and off as needed. When the relay was turned on, it triggered drive motor actuation. Observations were made on needle punching movement, cam and arm engagement, motor speed and structural vibration. Later, fiber web which composed of 70% bamboo fiber and 30% polyester fiber (4 denier) was fed into the prototype at fixed speed. Needle punching speed was adjusted to 60 rpm. Output felt visually inspected. This process continued by changing motor speed to 100 rpm, 150 rpm, 200 rpm and 300 rpm. Increasing the needle punching speed reducing the motor torque. This effected the punching force as described in Table 1 in previous section. Thus, it might influence the intertwining process of the fibers. Calculation on motor torque is summarized in Table 4. Each of the output felt were observed visually to investigate the fiber bonding properties.

#### 4. Result and Discussion

#### 4.1 Structural Analysis

The finite element analysis (FEA) simulation results displayed in the Table 4 showed variations in maximum stress, displacement, and strain across different simulations. As the simulation number increased, an overall upward trend in stress, displacement, and strain values was identified.

In the first simulation, the maximum recorded stress was  $1.836 \times 10^2 \,\mathrm{N/m^2}$ , with a displacement of  $1.486 \times 10^{-11} \,\mathrm{m}$  and a strain of  $1.995 \times 10^{-9}$ . With changes in loading conditions during the second simulation, the stress increased to  $5.097 \times 10^2 \,\mathrm{N/m^2}$ , while displacement and strain also rose to  $4.127 \times 10^{-11} \,\mathrm{m}$  and  $5.540 \times 10^{-9}$ , respectively. In the third simulation, stress continued to rise to  $1.147 \times 10^3 \,\mathrm{N/m^2}$ , accompanied by a displacement of  $9.282 \times 10^{-11} \,\mathrm{m}$  and strain of  $1.246 \times 10^{-8}$ .

A substantial increase in stress was noted in the fourth and fifth simulations, reaching  $2.038 \times 10^3 \,\text{N/m}^2$  and  $4.585 \times 10^3 \,\text{N/m}^2$ , respectively. Correspondingly, the displacement values grew to  $1.650 \times 10^{-10} \,\text{m}$  in the fourth simulation and  $3.712 \times 10^{-10} \,\text{m}$  in the fifth.

Similarly, strain values escalated to  $2.215 \times 10^{-8}$  and  $4.983 \times 10^{-8}$ , respectively.

The rising pattern in stress, displacement, and strain suggested that higher applied loads or modified boundary conditions in later simulations led to increased deformation and internal forces within the structure. These findings were crucial for assessing material behaviour, structural strength, and optimizing design performance under different loading scenarios.

Table 4: Result of stress, displacement and strain

Simulation No.	Maximum Stress (N/m²)	Maximum Displacement (m)	Maximum Strain
1	1.836 × E2	1.486 × E-11	1.995 × E-9
2	$5.097 \times E2$	$4.127 \times E-11$	$5.540 \times E-9$
3	$1.147 \times E3$	$9.282 \times E-11$	$1.246 \times E-8$
4	$2.038 \times E3$	$1.650 \times E-10$	$2.215 \times E-08$
5	$4.585 \times E3$	$3.712 \times E-10$	4.983 × E-8
Average	1692.66	1.3703 × E-10	1.8395 × E-8

The stress distribution mapping in the Fig. 6 represented the von Mises stress. As the speed increased, the stress concentration areas became more pronounced, particularly in the upper and central regions of the structure, where mechanical loading was most significant.

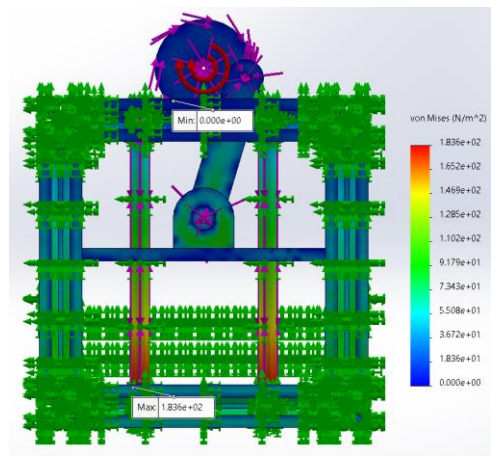


Fig. 6: Maximum stress distribution mapping on prototype

At 60 rpm, the stress distribution was relatively low, with the highest stress values observed near the rotating components and linkage mechanism. As the speed increased to 100 rpm, a noticeable rise in stress levels occurred, particularly in the uppermost section.

Next, at 150 rpm, stress levels further intensified, spreading to a larger portion of the structure. The central linkage area experienced increased stress due to higher inertial forces. By 200 rpm, stress concentration continued to grow, indicating that the structure endured greater mechanical loads.

The highest stress values were recorded at 300 rpm with increasing trend in stress concentration suggested that higher rotational speeds imposed greater forces on the structure, leading to elevated internal stresses. These results were crucial in evaluating the mechanical strength and stability of the system under different operating conditions.

#### 4.2 Functionality Test

There are few changes that have been made from the simulated design compared to the real model in Fig. 7. The reciprocating needle plate should be done using aluminium sheet but due the weight reduction purpose, it has been replaced with wooden plank to reduce the workforce to the gear motor and to provide more smooth reciprocation motion of the needle plate.

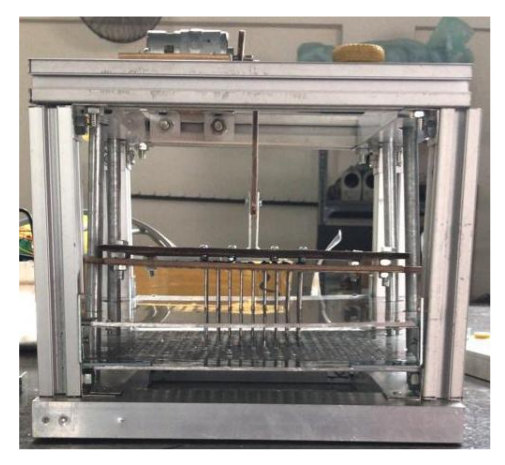


Fig. 7: Actual prototype setup

As shown in Table 5, five distinct fiber qualities were obtained through the application of varying motor speeds during the needle punching process. Notably, Sample A, which was subjected to a motor speed of 300 rpm, demonstrated the most refined fiber entanglement, characterized by a smoother and more homogeneous surface morphology.

During the needle punching process, fibers are mechanically entangled through the action of barbed needles. The repetitive penetration and withdrawal of the needles displace the fibers within the web, inducing interfiber contact. This interaction results in interfacial friction, which plays a fundamental role in promoting fiber bonding and entanglement. Oliveira et al. (2008) also mentioned, the forces exerted between fibers can significantly influence the extent of frictional entanglement, thereby impacting the overall structural cohesion and mechanical integrity of the non-woven fabric.

Then, at higher needle punching speeds, the increased kinetic energy and frequency of needle penetration enhance the intensity of frictional forces among the fibers. This elevated friction facilitates tighter fiber interlacement, greater compaction, and improved structural integrity of the resulting non-woven web. In contrast, lower punching speeds generate less dynamic interaction, thereby reduced fiber interlocking, yielding a less uniform and loosely bonded surface. As a result, the bonding becomes weaker, and the fiber arrangement appears less compact and more loosely structured. Roy & Ishtiaque (2019) clarified when needle punching speed increases, the velocity of the needles correspondingly increases. Given that kinetic energy is directly proportional to the square of velocity, this leads to a substantial increase in the kinetic energy imparted during each needle penetration.

Table 5: Result of specimen with different needle punching speed

Specimen	Motor Speed of Needle Punching (rpm)	Result of Specimen
A	60	S os os w us us
В	100	2 m m + m m
С	150	
D	200	
E	300	A 95 T 10 0

## 5. Conclusion and Recommendations

The design and development of a modular, small-scale needle punching non-woven machine prototype revealed tremendous possibilities for overcoming the operational constraints often associated with fiber testing in full-scale production environments. The major goal, which was to ease needle replacement and improve machine maintainability, was met through a compact modular architecture that assures accessibility and operating efficiency. Structural integrity was tested using finite element analysis, which revealed that stress, strain, and

displacement values stayed below permissible limits under varied operational loads, verifying the prototype framework's resilience and reliability. The prototype's operation was confirmed by experimental testing with a blend of untreated bamboo fiber and polyester, which resulted in optimum fiber entanglement and fabric homogeneity at a punching speed of 300 revolutions per minute. This demonstrated the system's capacity to create high-quality nonwoven fabrics while retaining consistent mechanical performance. The results also showed that increasing punching speed improved fiber interlocking due to increased frictional engagement, which supports the mechanical bonding mechanism inherent in the needle punching process. Based on these findings, future research should prioritize the use of advanced control systems, such as programmable speed feedback and real-time vibration monitoring, to improve dynamic stability. Furthermore, incorporating automated needle replacement mechanisms and conducting performance evaluations with a broader range of natural and recycled fibers could expand the prototype's applicability and reinforce its value as a sustainable and adaptable research platform in the nonwoven textile sector.

**Acknowledgement:** This research was fully supported by Universiti Tun Hussein Onn Malaysia (UTHM) through GPPS grant, Q594. The authors also would like to thank to Bambusoideae Technology Sdn. Bhd. for sponsoring raw materials for this project.

**Author Contributions:** The research study was carried out successfully with contributions from all authors. Raynabelle – Report writing, simulation analysis, Farid – Design and simulation, Yoga – Design and fabrication, Aqil – fabrication and testing, Aizat – Design, and Aimi – System setup.

**Conflicts of Interest:** The authors declare no conflict of interest.

#### References

- Ajmeri, J. R., & Ajmeri, C. J. (2016). Developments in nonwoven as geotextiles. In *Advances in technical nonwovens* (pp. 339-363). Woodhead Publishing. https://doi.org/https://doi.org/10.1016/B978-0-08-100575-0.00012-7.
- Albrecht, W., Fuchs, H., & Kittelmann, W. (Eds.). (2006). Nonwoven fabrics: raw materials, manufacture, applications, characteristics, testing processes. John Wiley & Sons.
- Ashby, M. F., & Jones, D. R. (2012). Engineering materials 1: an introduction to properties, applications and design (Vol. 1). Elsevier.
- Callister, W. D., & Rethwisch, D. (2018). Characteristics, applications, and processing of polymers. *Materials science and engineering: an introduction*, 8.

- Chapman, R. (Ed.). (2010). Applications of nonwovens in technical textiles. Elsevier.
- Hearle, J. W. (Ed.). (2001). *High-performance fibres*. Elsevier.
- Hill, C. (2019). The Science of Making Cotton. Springer.
- Hu, J. (2008). Introduction to three-dimensional fibrous assemblies.  $Hu\ J\ (ed)$ .
  - https://doi.org/10.1533/9781845694982.1.
- Huangfu, Z., Wang, J., Cheng, X., Feng, S., Liang, Y., Yuan, C., ... & Yang, K. (2023). The effect of different strain on the structural and optical properties of multilayer γ-InSe. *Journal of Alloys and Compounds*, 961, 170998.
  - https://doi.org/10.1016/J.JALLCOM.2023.170998.
- Kadolph, S. J., & Langford, A. L. (2002). *Textiles*. Pearson Education.
- Lawrence, C. A., & Branson, D. H. (2001). Nonwoven fabrics: A review. *Journal of Environmental Polymer Degradation*, 9(4), 187-202.
- Li, Q., Dai, G., & Zhang, Q. (2019). Structure and properties of bamboo fibers treated with high pressure steam. *Fibers and Polymers*, 20(1), 102-109.
- McDonagh, K. (2016). Textile Production and Consumption in the Ancient Mediterranean. In The Oxford Handbook of the Archaeology of Clothing and Textiles (pp. 31-50). Oxford University Press.
- Oliveira, M. H. D., Maric, M., & Ven, T. G. V. D. (2008). The role of fiber entanglement in the strength of wet papers. *Nordic Pulp & Paper Research Journal*, 23(4), 426-431.
- Oriental Motor U.S.A. Corp. (n.d.). *Motor sizing calculations*. Retrieved March 6, 2025 from https://surl.li/sjzpfb.
- Paul, P., Ahirwar, M., & Behera, B. K. (2022a). Acoustic behaviour of needle punched nonwoven structures produced from various natural and synthetic fibers. *Applied Acoustics*, 199, 109043.
  - https://doi.org/https://doi.org/10.1016/j.apacoust.2022. 109043.
- Paul, P., Ahirwar, M., & Behera, B. K. (2022b). Acoustic behaviour of needle punched nonwoven structures produced from various natural and synthetic fibers. *Applied Acoustics*, 199.
  - https://doi.org/10.1016/j.apacoust.2022.109043.
- Pourmohammadi, A. (2013). Nonwoven materials and joining techniques. In *Joining textiles* (pp. 565-581). Woodhead Publishing.
- Roy, R., & Ishtiaque, S. M. (2019). Influence of punching parameters on fibre orientation and related physical and mechanical properties of needle punched nonwoven. *Fibers and Polymers*, 20(1), 191-198. https://doi.org/10.1007/s12221-019-8784-4.
- Smith, A., & Jones, B. (2020). Advances in Synthetic Fiber Technology. *Journal of Materials Engineering*, 25(3), 112-130.

Takagi, S., & Yoshida, S. (2022). Development of estimation method for material property under high strain rate condition utilizing experiment and analysis. *International Journal of Pressure Vessels and Piping*, 199, 104771.

https://doi.org/10.1016/J.IJPVP.2022.104771.

Urone, P. P., & Hinrichs, R. (2016). 6.1 Rotation Angle and Angular Velocity. *College Physics*.

Xinhen. (n.d.). High speed needle punching machine-Jiangsu Xinhen Nonwoven Machinery Co.,Ltd. Retrieved June 26, 2023 from http://www.xinhennonwoven.com/productshow.asp?ID=48.